Metrologia

PAPER

Measurement of the $^{27}Al^{+}$ and ^{87}Sr absolute optical frequencies

IOP Publishing | Bureau International des Poids et Mesures Metrologia

Metrologia **58** (2021) 015017 (8pp) https://doi.org/10.1088/1681-7575/abd040

Measurement of the $^{27}Al^{+}$ and ^{87}Sr absolute optical frequencies

Holly Leopardi[1,2,3,*], Kyle Beloy[1], Tobias Bothwell[4], Samuel M Brewer[1,5,2], Sarah L Bromley[4,6], Jwo-Sy Chen[1,7,2], Scott A Diddams[1,2], Robert J Fasano[1,2], Youssef S Hassan[1,2], David B Hume[1], Dhruv Kedar[4], Colin J Kennedy[1,4], David R Leibrandt[1,2], Andrew D Ludlow[1], William F McGrew[1,2], William R Milner[4], Daniele Nicolodi[1,2,8], Eric Oelker[1,4], Thomas E Parker[1], John M Robinson[4], Stefania Romisch[1], Jeff A Sherman[1,*], Lindsay Sonderhouse[4], Jian Yao[1,4], Jun Ye[1,4], Xiaogang Zhang[1,2] and Tara M Fortier[1,2,*]

[1] National Institute of Standards and Technology, Boulder, CO 80305, United States of America
[2] Department of Physics, University of Colorado, Boulder, CO 80309, United States of America
[3] Space Dynamics Laboratory, Albuquerque, NM 87106, United States of America
[4] JILA, University of Colorado, Boulder, CO 80309, United States of America

E-mail: holly.leopardi@colorado.edu, jeff.sherman@nist.gov and tara.fortier@nist.gov

Received 17 September 2020, revised 4 November 2020
Accepted for publication 3 December 2020
Published 21 January 2021

Abstract

We perform absolute measurement of the $^{27}Al^{+}$ single-ion and ^{87}Sr neutral lattice clock frequencies at the National Institute of Standards and Technology and JILA at the University of Colorado against a global ensemble of primary frequency standards. Over an eight month period multiple measurements yielded the mean optical atomic transition frequencies $\nu_{Al^+} = 1\,121\,015\,393\,207\,859.50(0.36)$ Hz and $\nu_{Sr} = 429\,228\,004\,229\,873.19(0.15)$ Hz, where the stated uncertainties are dominated by statistical noise and gaps in the observation interval ('dead-time' uncertainty).

Keywords: optical frequency comb, atomic clocks, precision metrology, optical measurement, secondary standards

(Some figures may appear in colour only in the online journal)

1. Introduction

Atoms are excellent frequency references because identical copies exist in abundance, and because atoms behave as closed systems that naturally isolate clock transition frequencies from perturbations to external fields. For this reason, in 1967, the SI (International System of Units) second was defined as 9 192 631 770 cycles of the ground-state microwave hyperfine transition in ^{133}Cs. While the reduction of systematic uncertainties of microwave standards has enabled time to be defined with a resolution at 10^{-16}, trends in clock performance have slowed. In contrast, the performance, robustness and form-factor of optical atomic clocks have continued to progress. Optical clocks, which leverage 10^5 times higher carrier frequencies to achieve finer fractional measurement resolution, have been developed with control of systematic uncertainties at, and even below, the 10^{-18} level

* Authors to whom any correspondence should be addressed
[5] Current affiliation: Department of Physics, Colorado State University, Fort Collins, CO 80523, United States of America
[6] Current affiliation: Department of Physics, Durham University, Durham, United Kingdom.
[7] Current affiliation: IonQ, Inc, College Park, MD 20740, United States of America.
[8] Current affiliation: Physikalisch-Technische Bundesanstalt, Bundesallee 100, Braunschweig 38116, Germany.

a)

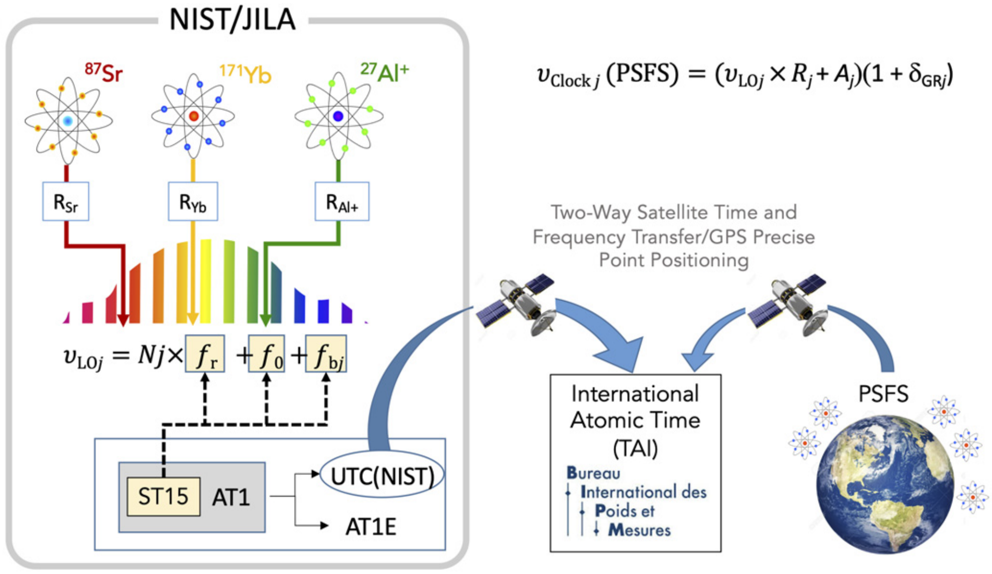

b)

Ratio	Relationship	Averaging Interval	Uptime/Duty-cycle
$\upsilon_{LOj}/ST15$	Measured mean frequency	1 s	< 1% (<10^5 s/month)
$ST15/AT1E$	Sampled phase difference	720 s	100 %
$AT1E/AT1$	Sampled phase difference	720 s	100 %
$AT1/UTC(NIST)$	Sampled phase difference/ Programmed frequency offset	720 s / 7 days	100 %
$UTC(NIST)/TAI$	Sampled phase difference	5 days	Hourly transmission $UTC(NIST)$ (< 2 % duty cycle)
$TAI/PSFS$	Measured mean frequency	25, 30, or 35 days	100 % (Circular T-month)

Figure 1. (a) Schematic of the frequency calibration chain connecting the optical transition frequencies of the $^{27}Al^+$, ^{87}Sr, and ^{171}Yb optical clocks to global PSFS via hybrid satellite and GPS microwave time/frequency links. The clock transition frequencies are coherently connected to LO via non-integer ratios, whereby $R_{Al^+} \sim 4$, $R_{Yb} \sim 2$ and $R_{Sr} \sim 1.1$, resulting in frequency relationships, $\nu_{clock\,j} \sim \nu_{LO_j}(PSFS) \times R_j$ (here j refers to the clock being measured). Optical interference between the LOs and the FLFC produces difference frequencies f_{b_j}, which along with the FLFC pulse repetition rate, f_r, and carrier-envelope-offset frequency, f_0, are detected and compared to the frequency of a single hydrogen maser (ST-15) in the NIST timescale [AT1, post-processed version AT1E, and steered output UTC(NIST)]. Calibration against PSFS occurs via transmission of UTC(NIST) to the BIPM in Paris, France. We account for local operational shifts on the optical clock transition frequencies, A_j, as well as a gravitational redshift correction, $\delta_{GR\,j}$, from the NIST and JILA laboratory altitude to the PSFS reference geopotential near sea level (see equation (3)). (b) Tabulation of the relationship, averaging intervals, and typical duty-cycles of each ratio link in this frequency calibration chain.

[1–4]. This 100-fold improvement in frequency uncertainty of optical clocks over microwave clocks heralds a future redefinition of the SI second based on optical transitions [5, 6].

In the meantime, optical clocks are employed as secondary representations of the second (SRS) to serve a number of important globally-realized metrological functions. The international organization of measurements standards, Bureau International des Poids et Mesures (BIPM), uses all available SRS measurements to periodically refine their recommended values of optical transition frequencies and to realize milestones required by the roadmap for the redefinition of the SI second [6]. Additionally, regular reporting of SRS observations by National Metrological Institutes (NMIs) help to reduce the realized instability and uncertainty of the International Atomic Timescale (TAI). In support of these efforts, here we report the absolute optical frequencies of the single-ion $^{27}Al^+$ clock, and the neutral ^{87}Sr lattice clock at NIST and JILA, with total measurement uncertainties below 4 parts in 10^{16}.

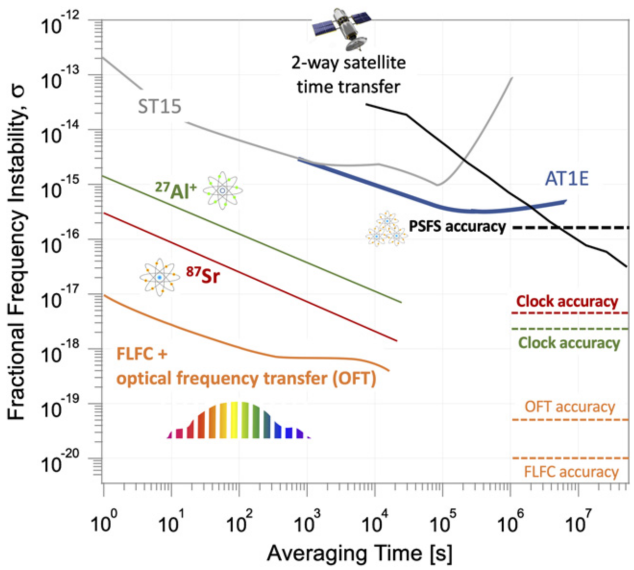

Figure 2. Comparison of the fractional frequency instability and the frequency accuracy of various frequency calibration chain elements in figure 1: ST-15 and AT1E [2], the $^{27}Al^+$, ^{87}Sr clocks, optical fiber links and FLFC [7], two-way satellite time/frequency transfer [8] and PSFS. For this work, PSFS defines the Hz unit; therefore PSFS's realized inaccuracy sets a lower bound on attainable optical clock frequency uncertainties [9].

2. Method

Figure 1 depicts the frequency calibration chain connecting the NIST $^{27}Al^+$, ^{87}Sr, and ^{171}Yb optical clocks to the global ensemble of primary- and secondary-frequency standards (PSFS). For a depiction of the stability and accuracy limitations of the various frequency calibration chain elements in figure 1, please consult figure 2. It is important to note that this work shares the experimental setup and measurement system used for remote calibration of the ^{171}Yb optical clock to PSFS [2]. Additionally, many of the measurement days described here overlapped with those during the direct optical clock ratio measurements detailed in reference [7]. While reference [2] details the measurement of ^{171}Yb with respect to PSFS, here we extend our analysis to the absolute frequencies of the $^{27}Al^+$ and ^{87}Sr clocks and provide additional details regarding the microwave frequency counting accuracy.

2.1. Generation and transport of optical atomic clock signals

The ^{87}Sr, ^{171}Yb, and $^{27}Al^+$ [1, 3, 10] atomic clocks are based on doubly forbidden $^1S_0 \leftrightarrow ^3P_0$ electronic transitions. Laser-based frequency synthesis coherently connects the ^{87}Sr, ^{171}Yb, and $^{27}Al^+$ transition frequencies near 429 THz, 518 THz, and 1.1 PHz to local oscillators (LOs) near 194 THz, 259 THz, and 280 THz, respectively. The LOs are laser-stabilized to high-performance Fabry–Perot cavities (e.g. [11]) that are made resonant with the atomic clock transition frequencies using acousto-optic modulators as additive frequency shifters. Harmonics of the LOs are used to probe ^{171}Yb and $^{27}Al^+$, where in the case of ^{87}Sr, the LO is translated to the atomic resonance by a dedicated femtosecond laser frequency comb (FLFC) [3]. While ^{171}Yb and $^{27}Al^+$ clocks are located at NIST-Boulder, the ^{87}Sr clock is located approximately 1.5 km away at JILA, on the University of Colorado campus. The three atom-stabilized LO signals are delivered via Doppler-cancelled [12, 13] optical fiber links (50 m to 1.5 km) to an FLFC at NIST, with link instability of approximately $1 \times 10^{-17}(\tau/1\ \mathrm{s})^{-1/2}$ [7] (see figure 2), where τ represents the averaging time. More specifically, the 194 THz LO light delivered from the JILA Sr lab is amplified and frequency doubled, at NIST, to 389 THz so as to be accessible by the FLFC that performs the optical-to-microwave division.

2.2. Optical-to-microwave division of atomic clock signals

When phase-locked to an atomic reference, an FLFC transfers that reference's stability and accuracy to evenly spaced frequency modes across an optical octave of bandwidth [14]. This coherent synthesis permits simultaneous frequency comparison of multiple atomic clocks with an additive fractional instability of $<1 \times 10^{-17}(\tau/1\ \mathrm{s})^{-1/2}$ [7], and additive uncertainty below 1 part in 10^{19} [15–19]. Here, a home-built mode-locked octave-spanning Ti:sapphire FLFC [20] converts the optical clock signals to the microwave domain for comparison against microwave standards. Direct photodetection of the stable FLFC optical pulse train produces the optical mode spacing, f_r, as a microwave signal. Optical clock LO frequencies are linked to f_r and two other microwave frequencies via the following relationship:

$$\nu_{\mathrm{LO}_j} = N_j f_\mathrm{r} + f_0 + f_{\mathrm{b}_j}. \tag{1}$$

Other than N_j, an integer $\sim 10^5$, all terms on the right-hand side of equation (1) are microwave signals with frequencies near or below 1 GHz. Here, f_{b_j} measures the optical frequency difference between a clock's LO, ν_{LO_j} and a single optical FLFC mode, $\nu_\mathrm{N} = N \times f_\mathrm{r} + f_0$. For the measurements performed here, the FLFC was phase locked to the ^{171}Yb clock LO via $f_{\mathrm{b}_{\mathrm{Yb}}}$. A self-referenced stabilization scheme [21–23] permits measurement and stabilization of the FLFC carrier-envelope-offset frequency, f_0, and high-fidelity optical synthesis across an octave of bandwidth (550 nm to 1100 nm) with an additive instability below 1×10^{-17} for times greater than 1 s [7]. Both f_0 and $f_{\mathrm{b}_{\mathrm{Yb}}}$ heterodyne beat signals were stabilized to microwave references derived from a single H-maser, ST-15. In this configuration, the FLFC divides the optical reference frequency by approximately 10^5 to the microwave domain [24, 25]; the output is realized as the FLFC mode spacing, $f_\mathrm{r} \approx 1$ GHz. Comparison of another optical clock j to a microwave standard is achieved by measuring the beat signal f_{b_j} in equation (1) with a high-resolution frequency counter (here, an Agilent 53132A [9]). For consistency, all synthesizers and frequency counters used by the optical atomic clock systems and the FLFC were referenced to the same maser source, ST-15.

[9] Mention of specific products does not constitute an endorsement by the National Institute of Standards and Technology.

2.3. NIST microwave ensemble timescales

ST-15 is one of about 12 H-masers in the free-running NIST microwave ensemble timescales, AT1 and AT1E. The phase difference of ST-15 with respect to both timescales is calculated on a regular 12 minute (720 s) observation grid. AT1E is a post-processed timescale that uses the same algorithm as AT1 but can achieve slightly higher stability since members with irregular frequency deviations (e.g., due to temporary loss of environmental control) can have their statistical weight attenuated 'before' they adversely influence the ensemble. AT1, however, is computed in realtime to realize broadcast signals. Consequently, the frequency of ST-15 is first compared against AT1E due to its higher stability, where the average frequency offset between AT1E and AT1 is separately analyzed [2].

2.4. Frequency calibration chain from NIST to PSFS

Programmed frequency offsets are applied (typically weekly) to AT1 to create UTC(NIST), a physical signal synthesized from an ensemble member clock, which is broadcast to the BIPM in Paris using a hybrid two-way satellite time and frequency transfer/GPS precise point positioning frequency transfer protocol (TWSTFT/GPSPPP) [26–28]. The link allows frequency measurement of UTC(NIST) against TAI. Finally, the rate of TAI is calibrated monthly against the ensemble of atomic references, PSFS. Both of these comparisons are published in the BIPM journal, Circular T [29].

Using the frequency chain described above, the absolute frequency of optical clock j, $\nu_{\mathrm{Clock}\,j}(\mathrm{PSFS})$, as calibrated against PSFS can be expressed as a product of measurement ratios in the frequency chain described above:

$$\frac{\nu_{\mathrm{Clock}\,j}}{1\ \mathrm{Hz}} = \frac{\nu_{\mathrm{Clock}\,j}}{\mathrm{ST}-15} \times \frac{\mathrm{ST}-15}{\mathrm{AT1E}} \times \frac{\mathrm{AT1E}}{\mathrm{AT1}} \times \frac{\mathrm{AT1}}{\mathrm{UTC(NIST)}} \times \frac{\mathrm{UTC(NIST)}}{\mathrm{TAI}} \times \frac{\mathrm{TAI}}{\mathrm{PSFS}}. \tag{2}$$

3. Results

We measured the optical clocks intermittently over eight months (November 2017 to June 2018). The campaign included 16 measurements of $^{27}\mathrm{Al}^+$ and 11 measurements of $^{87}\mathrm{Sr}$. The measurement durations ranged from 10^3 s to 10^5 s and the measurements were nearly-continuous, but were separated by periods of dead time extending from days to months. Concatenating all measurements, the total observation durations were 168 000 s and 212 000 s, for $^{27}\mathrm{Al}^+$ and $^{87}\mathrm{Sr}$, respectively. Table 1 summarizes the type A and B uncertainties for the reported measurements. While we discuss the limiting uncertainties here, a more detailed discussion is found in section 4.

As seen in figure 2, optical systems that leverage higher carrier frequencies, including the clocks, the FLFC and fiber optic time/frequency transfer contribute negligible instabilities and inaccuracies as compared with the lower frequency microwave references, time transfer and measurement systems. Based on the high overlap in measurement days between the results presented here and our recent optical ratio measurements, we discern a statistical measurement uncertainty at the low 10^{-18} level for both optical clocks over the total measurement campaign [7]. In comparison, as a result of the higher short-term instability, the NIST microwave timescale yielded statistical uncertainties just slightly below 1×10^{-16}. Due to the low operational duty cycle of the clocks and the frequency drift of AT1E (<1% over an average Circular T month), there is an additional 'dead-time' uncertainty of 2.4×10^{-16} for $^{27}\mathrm{Al}^+$, and 2.6×10^{-16} for $^{87}\mathrm{Sr}$, respectively. A detailed treatment of the dead-time calculation can be found in [2]. The next largest source of uncertainty resulted from the instability of intercontinental time- and frequency-transfer linking UTC(NIST) to TAI. As illustrated in figure 2, TWSTFT/GPSPPP requires more than one month of averaging to match an optical clock's instability over a few minutes of averaging [26]. The high transfer uncertainty in TWSTFT [8] results from a combination of low transmission up-times of approximately 2 min every 2 h, non-reciprocal delays in transmission through the ionosphere [33, 34], and environmental susceptibility and aging of the transfer equipment. As seen in table 1, the transfer uncertainty for the $^{27}\mathrm{Al}^+$ and $^{87}\mathrm{Sr}$ clock measurements were 1.1×10^{-16} and 1.5×10^{-16}, respectively.

Table 1 summarizes the type A and B uncertainties for the reported measurements. Type A uncertainties encompass all

Table 1. Standard fractional uncertainties in the frequency comparison of the NIST $^{27}\mathrm{Al}^+$ and $^{87}\mathrm{Sr}$ clocks to the global ensemble PSFS. The optical systems, including the optical clocks [3, 10] and FLFC, contributed negligible type A and B uncertainties. The two largest uncertainty contributions result from dead-time uncertainty and frequency transfer uncertainty. The total type A and B uncertainties are the quadrature sum of type A and B components, respectively. The total uncertainty of the absolute frequency measurement for each optical clock is determined from the quadrature sum of type A and B contributions.

	$^{27}\mathrm{Al}^+$	$^{87}\mathrm{Sr}$
Type an uncertainties ($\times 10^{-16}$)		
Dead time	2.4	2.6
Frequency transfer	1.1	1.5
Measurement statistics	0.9	0.8
Time scale	0.03	0.02
FLFC/optical clock	<0.01	<0.01
PSFS	0.7	0.9
Type A total	2.9	3.3
Type B uncertainties ($\times 10^{-16}$)		
Frequency counting/synthesis	0.3	0.3
FLFC	<0.001	<0.001
PSFS	1.2	1.3
Optical clock	<0.1	<0.1
Gravitational redshift	0.6	0.6
Type B total	1.4	1.5
Total uncertainty	3.2	3.6

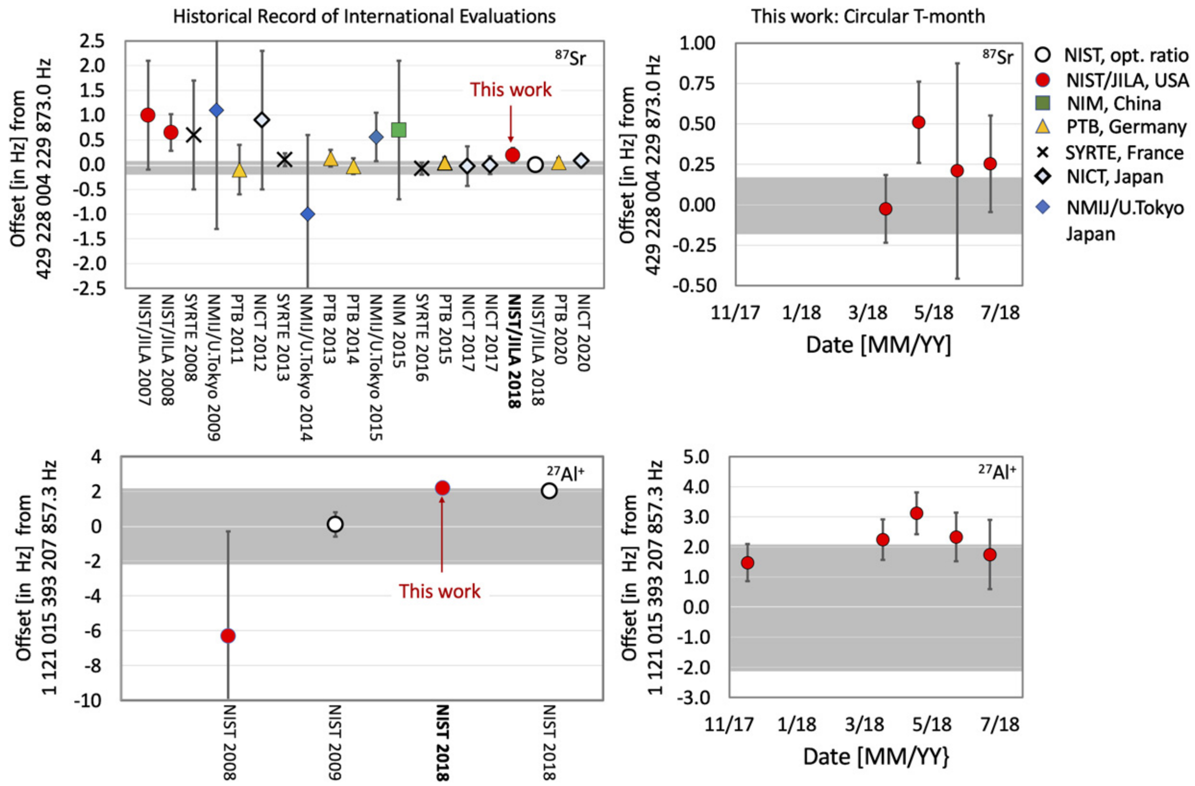

Figure 3. Comparison of internationally reported values for the optical frequencies of $^{27}\mathrm{Al}^+$, and $^{87}\mathrm{Sr}$. Points are color coded by country; error bars depict each measurement's standard uncertainty. All points are represented as offset in hertz from the indicated 2017 BIPM recommended transition frequencies. The gray bands illustrate the stated uncertainty for each 2017 BIPM recommended value. 'This work' in the left hand plots is represented by the weighted mean of the Circular T monthly observations shown separately in the right hand plots. Also depicted as empty circles are the absolute frequencies for $^{27}\mathrm{Al}^+$ and $^{87}\mathrm{Sr}$ as calculated from our most recent optical ratio measurement [7] and our most recent absolute frequency evaluation of $^{171}\mathrm{Yb}$ via remote comparison against PSFS [2]. References to all data points aside from those in 2020 and 2018 can be found at the BIPM website, listed in reference [30]. The most recent 2020 $^{87}\mathrm{Sr}$ data from the PTB in Germany and NICT in Japan can be found in references [31, 32].

known effects for which the distribution of values are known from repeated collection of data, for example, uncertainties due to statistical effects. Type B uncertainties are effects for which the distribution of uncertainty is indirectly inferred from prior information. The total measurement uncertainties, calculated as the quadrature sum of the type A and B uncertainties in table 1, were found to be 3.2×10^{-16} and 3.6×10^{-16} for $^{27}\mathrm{Al}^+$ and $^{87}\mathrm{Sr}$, respectively. It is important to note that the lowest uncertainty attainable is set by the realized accuracy of PSFS [9], which is determined monthly by the global ensemble of independent frequency references reported by NMIs via TWSTFT/GPSPPP to Europe [35]. The PSFS uncertainty includes an appropriate weighted average of ensemble members' statistical and type B uncertainties, as well as their corresponding dead-time and time-transfer uncertainties. For the $^{27}\mathrm{Al}^+$ and $^{87}\mathrm{Sr}$ measurements here, we report the weighted mean of results averaged over Circular T month intervals. The monthly results are weighted according to the inverse-square of their estimated total uncertainties to obtain the absolute frequency results:

$$\nu_{\mathrm{Al}^+}(\mathrm{PSFS}) = 1\,121\,015\,393\,207\,859.50(0.36)\,\mathrm{Hz}$$

$$\nu_{\mathrm{Sr}}(\mathrm{PSFS}) = 429\,228\,004\,229\,873.19(0.15)\,\mathrm{Hz}$$

Figure 3 compares these values to previously reported results where all results are depicted as offset in hertz from the current BIPM recommended values, $\nu_{\mathrm{Al}^+}^{\mathrm{BIPM17}} = 1\,121\,015\,393\,207\,857.3(2.1)\mathrm{Hz}$ and $\nu_{\mathrm{Sr}}^{\mathrm{BIPM17}} = 429\,228\,004\,229\,873.0(0.17)$ Hz. By comparing our current results to the 2017 recommended frequency standard values, we find agreement within 1.02σ and 0.83σ for the $^{27}\mathrm{Al}^+$ and $^{87}\mathrm{Sr}$ values, respectively, where σ is the standard uncertainty. While the $^{87}\mathrm{Sr}$ clock has a rich history of measurement by many other NMIs [6], the only previous absolute frequency determination of $^{27}\mathrm{Al}^+$ was obtained in 2008 [36]. The second evaluation of $^{27}\mathrm{Al}^+$ in 2009 was made via optical ratio measurement against $^{199}\mathrm{Hg}^+$, which accounts for the smaller measurement uncertainty. Comparing our absolute frequency results from 2008 $^{27}\mathrm{Al}^+$ to the one made here yields a 2.7σ discrepancy.

The highest accuracy absolute measurement of $^{87}\mathrm{Sr}$ (1.5 parts in 10^{16}) has recently been realized by the Physikalisch-Technische Bundesanstalt (PTB) group in Germany by averaging data taken from 2017 to 2019 [31]. We find agreement between this result and our own to within 1.25σ. Also shown in figure 3, depicted as empty circles, are the calculated absolute frequencies of $^{27}\mathrm{Al}^+$, $\nu_{\frac{\mathrm{Al}}{\mathrm{Yb}}*\mathrm{Yb(PSFS)}} =$

1 121 015 393 207 859.33(0.24) Hz and ^{87}Sr, $\nu_{\frac{\mathrm{Sr}}{\mathrm{Yb}}*\mathrm{Yb(PSFS)}} =$ 429 228 004 229 873.06(0.09) Hz. These values were calculated from our most recent optical ratio measurements of ^{171}Yb/^{87}Sr and ^{27}Al^{+}/^{171}Yb [7] and our most recent remote absolute frequency evaluation of ^{171}Yb to PSFS [2]. These frequencies calculated via direct optical ratio measurement and the absolute measured values evaluated here yield loop misclosures, $1 - \frac{\mathrm{PSFS}}{^{27}\mathrm{Al}^{+}} \times \frac{^{171}\mathrm{Yb}}{\mathrm{PSFS}} \times \frac{^{27}\mathrm{Al}^{+}}{^{171}\mathrm{Yb}} = (1.59 \pm 3.8) \times 10^{-16}$ and $1 - \frac{\mathrm{PSFS}}{^{87}\mathrm{Sr}} \times \frac{^{171}\mathrm{Yb}}{\mathrm{PSFS}} \times \frac{^{87}\mathrm{Sr}}{^{171}\mathrm{Yb}} = (3.09 \pm 4.17) \times 10^{-16}$.

4. Frequency chain uncertainties

4.1. Optical clock uncertainties

Two parameters must be calculated to connect each clock's laboratory LO laser frequency to the ideal atomic transition frequency (i.e. perturbation-free, at rest, in a 0 K thermal environment). The first is a ratio, R_j, which translates clock j's LO to its atomic transition frequency as realized in the laboratory. The second parameter, A_j accounts for known perturbations and field shifts that cause the transition frequency to deviate from ideal conditions. The ratio, R_j, includes frequency multiplication stages (in this work the laser LOs are infrared, whereas the atomic transition frequencies are visible or ultraviolet), as well as additive shifts from the Doppler-cancelled fiber links and feedback loops. For ^{27}Al^{+} and ^{87}Sr, R_j are non-integers near 4 and 1.1, respectively. A_j is generally a time-dependent parameter, resulting in a fractional frequency shift ranging from (1 to 5) $\times 10^{-15}$ for each clock. For this work, the optical clocks were operated with control of these field-related shifts all with uncertainties below 5×10^{-18}. Details pertaining to the measurement of the systematic shifts on the atomic transitions can be found in references [1–3].

4.2. Geopotential uncertainty

The optical clocks and measurement system were operated roughly 1647 m above sea level, whereas PSFS is defined at a reference geopotential coincident with Earth's rotating geoid. Together with the terms R_j and A_j described above, a correction for the gravitational redshift $\delta_{\mathrm{GR}j} = g * \Delta h/c^2$ is required to connect the measured LO laser frequencies to PSFS-referenced measurements of the ideal atomic clock transition frequencies. Here c is the speed of light, g is the gravitational acceleration due to the earth's potential, and Δh is the altitude difference between two time reference planes. For an altitude correction from Boulder altitude to sea level, $\delta_{\mathrm{GR}}j \approx 1.8 \times 10^{-13}$. As a result, clock absolute frequencies can be expressed as,

$$\nu_{\mathrm{Clock}_j}(\mathrm{PSFS}) = (R_j \times \nu_{\mathrm{LO}} + A_j)(1 + \delta_{\mathrm{GR}_j}). \qquad (3)$$

Here, time dilation due to the gravitational redshift was treated separately from the clock operational shifts A_j because it is common to each clock at the 10^{-16} level. This is in contrast to the clock systematic shifts, which are clock dependent. While geopotential measurements have been made locally with uncertainties in relative altitude between clocks at NIST and JILA below 1 cm [7, 37], or near parts in 10^{18}, uncertainties in coastal leveling accumulate to about 1 m at our laboratories, meaning that $\delta_{\mathrm{GR}j}$ contributes uncertainty at 0.6×10^{-16} [38].

4.3. Frequency counter measurement uncertainties

We used commercial (Λ-type) frequency counters to measure all microwave beatnote frequencies generated by the interference between clock LOs and the FLFC. The timebases of all counters were referenced to 10 MHz maser signals from a single distribution amplifier. Tests were performed throughout the campaign, where each counter measured the same 10 MHz source as its timebase reference. From measurements averaged over 10^5 s, all counters used in our measurements revealed systematic biases of magnitude $\delta\epsilon_c \leqslant 3 \times 10^{-12}(\tau_{\mathrm{g}}/1\ \mathrm{s})^{-1}$, where $\tau_{\mathrm{g}} > 1$ s is the counter 'gating' interval. From the same measurements we also discerned that the counters contributed a measurement instability of $< 10^{-11}\tau^{-1/2}$, yielding greater than 11 digits of frequency resolution at $\tau_{\mathrm{g}} = 1$ s.

For signals that are additive offsets to optical frequencies (f_0 and f_{b_j}), counter biases contribute a fractional error to the optical clock frequencies of

$$\sigma_{y,c} = \delta\epsilon_c \times \frac{f_{\mathrm{input}}}{\nu_{\mathrm{LO}_j}}, \qquad (4)$$

where f_{input} is measured directly by the counter and ν_{LO_j} is an optical LO frequency; favorably, these form a small ratio. Conservatively, assuming the largest observed counter offset $\delta\epsilon_c = 3 \times 10^{-12}$, $f_{\mathrm{input}} = f_{\mathrm{b}_j} = 640$ MHz (the highest frequency employed), and $\nu_{\mathrm{LO}_j} = 194$ THz, the resulting error is bounded by $\sigma_{y,c} = 1 \times 10^{-17}$.

Counter errors on the FLFC pulse repetition rate f_{r} afford no such microwave-to-optical suppression on the ratio. Counter biases contribute a fractional error to optical clock frequencies,

$$\sigma_{y,c} = \delta\epsilon_c \times \frac{f_{\mathrm{input}}}{f_{\mathrm{r}}} \approx \delta\epsilon_c \times \frac{N_j f_{\mathrm{r}}}{\nu_{\mathrm{LO}_j}}, \qquad (5)$$

where in the last expression we set $f_{\mathrm{input}} = f_{\mathrm{r}}$ and recall that $N_j > 10^5$.

To minimize the counter errors for $f_{\mathrm{r}} = 1\ \mathrm{GHz} - \Delta$, where $\Delta < 400$ kHz, the repetition rate was mixed with a 1 GHz signal synthesized via multiplication of ST-15 by 200 permitting counting of a frequency <1 MHz. The difference frequency, Δ, was input into an ST-15-referenced counter whose fractional error was evaluated to be $\delta\epsilon_c \approx 2 \times 10^{-13}$, the lowest measured offset for any of our counters. Since the counter bias scales inversely with τ_{g}, we reduce the bias's effect on determination of f_{r} by operating with $\tau_{\mathrm{g}} = 10$ s. This operating configuration suppresses the counting error for a 194 THz carrier to below 1 part in 10^{17}. Frequency multiplication errors of the ST-15 10 MHz signals to 1 GHz bounded additional offsets at $<3 \times 10^{-17}$.

A secondary check of the additive counter biases was obtained using a software defined radio (SDR)-based counter [39] that measured f_{r} in parallel with the Λ-type counter.

The SDR measures the evolving phase difference of the input signal with respect to the reference to produce a zero dead-time frequency measurement once per second with a software acquisition rate of 1 MHz and a 50 Hz equivalent noise bandwidth achieved using a software digital filter. To do this, the SDR operates in two-channel differential mode whereby Δ is input into one digitizer channel and the 10 MHz ST-15 reference is input into a second digitizer and also stabilizes the digitizers' 100 MHz sampling/logic clock. Residual analysis showed the SDR counter contributed fractional offsets of $\sigma_{y,\mathrm{SDR}} < 1 \times 10^{-17}$ on a f_{r} of 1 GHz (dominated by a turn-on transient). The SDR data was gated asynchronously with that of the Λ-type counter, providing an independent measurement of f_{r}, and with agreement realized to within the statistical noise. The total type B fractional uncertainty including contributions from microwave synthesis and counting were found to contribute 3×10^{-17} toward absolute optical frequency measurements. The largest contributor was found to be frequency multiplication of ST-15 to 1 GHz as determined via residual phase measurement using the SDR.

5. Conclusions

We described the methods and frequency calibration chain used in the measurements of the absolute transition frequencies of the ^{87}Sr and ^{27}Al^{+} optical clocks at NIST, Boulder. While measurements obtained against PSFS permit a lower total uncertainty compared to those using a single, local ^{133}Cs primary standard, there are two significant drawbacks related to higher statistical (type A) uncertainties. First, the longer measurement duration required to average down the frequency instability in the TWSTFT/GPSPPP time-transfer links yielded a transfer uncertainty near 1 part in 10^{16}. Second, calibration against PSFS necessitates averaging over a Circular T month, whereby low optical measurement duty cycle yields an extra statistical 'dead-time' noise equivalent to an uncertainty near 2.5×10^{-16} for both optical clocks. Despite these limiting sources of uncertainty, periodic evaluation over an eight month period yielded a total fractional measurement uncertainty of 3.6×10^{-16} and 3.2×10^{-16} for the ^{87}Sr and ^{27}Al^{+} clocks, respectively. While our realized measurement uncertainty is close to the accuracy limit of primary atomic standards and represents an important step toward redefinition of the SI second [6], uncertainties due to coastal leveling and microwave time/frequency transfer between distantly located clocks represent a significant hurdle for realizing improved timing uncertainty below parts in 10^{-16} even as the SI second moves toward redefinition to optical atomic time.

Acknowledgments

The authors acknowledge NIST for funding this project. H Leopardi acknowledges funding from the National Defense Science and Engineering Graduate (NDSEG) Fellowship (32 CFR 168a). We would like to thank N Nardelli, C Oates and R Brown for careful reading of the manuscript and V Zhang for helpful conversations regarding TWSTFT/GPSPPP instability and noise. A Ludlow acknowledges funding from the National Aeronautics and Space Administration (NASA) and The Defense Advanced Research Projects Agency (DARPA). C J Kennedy and E Oelker acknowledge support from NRC Fellowship. The work at JILA is supported by DARPA, NIST, and NSF PHY-1734006.

ORCID iDs

Tobias Bothwell https://orcid.org/0000-0002-9532-1290
Daniele Nicolodi https://orcid.org/0000-0003-1467-1756
Tara M Fortier https://orcid.org/0000-0003-2282-4986

References

[1] Brewer S M, Chen J-S, Hankin A M, Clements E R, Chou C W, Wineland D J, Hume D B and Leibrandt D R 2019 ^{27}Al^{+} quantum-logic clock with a systematic uncertainty below 10^{-18} *Phys. Rev. Lett.* **123** 033201

[2] McGrew W F *et al* 2019 Towards the optical second: verifying optical clocks at the SI limit *Optica* **6** 448–54

[3] Bothwell T, Kedar D, Oelker E, Robinson J M, Bromley S L, Tew W L, Ye J and Kennedy C J 2019 JILA SrI optical lattice clock with uncertainty of 2.0×10^{-18} *Metrologia* **56** 065004

[4] Nicholson T L *et al* 2015 Systematic evaluation of an atomic clock at 2×10^{-18} total uncertainty *Nat. Commun.* **6** 6896

[5] Gill P 2016 Is the time right for a redefinition of the second by optical atomic clocks? *J. Phys.: Conf. Ser.* **723** 012053

[6] Riehle F, Gill P, Arias F and Robertsson L 2018 The CIPM list of recommended frequency standard values: guidelines and procedures *Metrologia* **55** 188–200

[7] Beloy K *et al* (Boulder Atomic Clock Optical Network and Collaboration) 2020 Frequency ratio measurements with 18-digit accuracy using a network of optical clocks (arXiv:2005.14694) in review 2020)

[8] Panfilo G and Parker T E 2010 A theoretical and experimental analysis of frequency transfer uncertainty, including frequency transfer into TAI *Metrologia* **47** 552–60

[9] Panfilo G and Arias F 2019 The coordinated universal time (UTC) *Metrologia* **56** 042001

[10] McGrew W F *et al* 2018 Atomic clock performance enabling geodesy below the centimetre level *Nature* **564** 87–90

[11] Matei D G *et al* 2017 1.5 μm lasers with sub-10 mHz linewidth *Phys. Rev. Lett.* **118** 1–6

[12] Ma L-S, Jungner P, Ye J and Hall J L 1994 Delivering the same optical frequency at two places: accurate cancellation of phase noise introduced by an optical fiber or other time-varying path *Opt. Lett.* **19** 1777–9

[13] Foreman S M, Holman K W, Hudson D D, Jones D J and Ye J 2007 Remote transfer of ultrastable frequency references via fiber networks *Rev. Sci. Instrum.* **78** 021101

[14] Fortier T and Baumann E 2019 20 years of developments in optical frequency comb technology and applications *Commun. Phys.* **2** 1–16

[15] Ma L-S *et al* 2004 Optical frequency synthesis and comparison with uncertainty at the 10^{-19} level *Science* **303** 1843–5

[16] Ma L-S *et al* 2007 Frequency uncertainty for optically referenced femtosecond laser frequency combs *IEEE J. Quantum Electron.* **43** 139

[17] Yao Y, Jiang Y, Yu H, Bi Z and Ma L 2016 Optical frequency divider with division uncertainty at the 10^{-21} level *Natl Sci. Rev.* **3** 463–9

[18] Leopardi H, Davila-Rodriguez J, Quinlan F, Olson J, Sherman J A, Diddams S A and Fortier T M 2017 Single-branch Er: fiber frequency comb for precision optical metrology with 10^{-18} fractional instability *Optica* **4** 879

[19] Johnson L A M, Gill P and Margolis H S 2015 Evaluating the performance of the NPL femtosecond frequency combs: agreement at the 10^{-21} level *Metrologia* **52** 62

[20] Fortier T M, Bartels A and Diddams S A 2006 Octave-spanning Ti:sapphire laser with a repetition rate >1 GHz for optical frequency measurements and comparisons *Opt. Lett.* **31** 1011–3

[21] Reichert J, Holzwarth R, Udem T and Hänsch T W 1999 Measuring the frequency of light with mode-locked lasers *Opt. Commun.* **172** 59–68

[22] Telle H R, Steinmeyer G, Dunlop A E, Stenger J, Sutter D H and Keller U 1999 Carrier-envelope offset phase control: a novel concept for absolute optical frequency measurement and ultrashort pulse generation *Appl. Phys.* B **69** 327–32

[23] Jones D J, Diddams S A, Ranka J K, Stentz A, Windeler R S, Hall J L and Cundiff S T 2000 Carrier-envelope phase control of femtosecond mode-locked lasers and direct optical frequency synthesis *Science* **288** 635–9

[24] Bartels A, Diddams S A, Oates C W, Wilpers G, Bergquist J C, Oskay W H and Hollberg L 2005 Femtosecond-laser-based synthesis of ultrastable microwave signals from optical frequency references *Opt. Lett.* **30** 667–9

[25] Fortier T M *et al* 2011 Generation of ultrastable microwaves via optical frequency division *Nature Photon.* **5** 425–9

[26] Parker T E 2012 Invited review article: the uncertainty in the realization and dissemination of the SI second from a systems point of view *Rev. Sci. Instrum.* **83** 1–7

[27] Petit G, Arias F and Panfilo G 2015 International atomic time: status and future challenges *C. R. Phys.* **16** 480–8

[28] Jiang Z and Petit G 2009 Combination of TWSTFT and GNSS for accurate UTC time transfer *Metrologia* **46** 305–14

[29] BIPM Circular T: monthly http://bipm.org/jsp/en/TimeFtp.jsp

[30] BIPM recommended values of standard frequencies https://bipm.org/en/publications/mises-en-pratique/standard-frequencies.html

[31] Schwarz R *et al* 2020 Long term measurement of the ^{87}Sr clock frequency at the limit of primary Cs clocks *Phys. Rev. Research* **2** 033242

[32] Nemitz N, Gotoh T, Nakagawa F, Ito H, Hanado Y, Ido T and Hachisu H 2020 Absolute frequency of ^{87}Sr at 1.8×10^{-16} uncertainty by reference to remote primary frequency standards *Metrologia* Accepted

[33] Petit G and Defraigne P 2016 The performance of GPS time and frequency transfer: comment on 'a detailed comparison of two continuous GPS carrier-phase time transfer techniques' *Metrologia* **53** 1003–8

[34] Lee S W, Schutz B E, Lee C-B and Yang S H 2008 A study on the common-view and all-in-view GPS time transfer using carrier-phase measurements *Metrologia* **45** 156–67

[35] Petit G and Panfilo G 2013 Comparison of frequency standards used for TAI *IEEE Trans. Instrum. Meas.* **62** 1550–5

[36] Rosenband T *et al* 2008 Frequency ratio of Al^+ and Hg^+ single-ion optical clocks; metrology at the 17th decimal place *Science* **319** 1808–12

[37] Westrum V 2019 Geodetic survey of NIST and JILA clock laboratories *NOAA Technical Memorandum* NOS NGS 77

[38] Pavlis N K and Weiss M A 2017 A re-evaluation of the relativistic redshift on frequency standards at NIST, boulder, Colorado, USA *Metrologia* **54** 535–48

[39] Sherman J A and Jördens R 2016 Oscillator metrology with software defined radio *Rev. Sci. Instrum.* **87** 054711